



# Tunable Color Emissions upon UV Irradiation from Tb<sup>3+</sup>:Y<sub>2</sub>SiO<sub>5</sub> Phosphor

Vijay Singh<sup>1</sup> · M. Seshadri<sup>2</sup> · M. Radha<sup>3</sup> · Chaitali M. Mehare<sup>4</sup> · S. J. Dhoble<sup>4</sup> · Ji Bong Joo<sup>1</sup>

Received: 22 August 2023 / Accepted: 7 February 2024 / Published online: 14 March 2024  
© The Minerals, Metals & Materials Society 2024

## Abstract

A series of terbium-activated yttrium oxyorthosilicate (Tb<sup>3+</sup>:Y<sub>2</sub>SiO<sub>5</sub>) phosphor was prepared through the sol–gel technique at a high calcination temperature of 1100°C. The phase purity was examined by the x-ray diffraction (XRD) analysis and found to be X1 type for all series of samples. The existence of functional groups in the prepared samples was confirmed by Fourier-transform infrared (FT-IR) spectroscopy. The sample exhibited absorption bands of Si-O-Si and Y-O groups at wavenumbers between 717 cm<sup>-1</sup> and 550 cm<sup>-1</sup>, and the NO<sub>3</sub> groups appeared between 800 cm<sup>-1</sup> and 1020 cm<sup>-1</sup> in the FT-IR spectra. Under 244-nm excitation, the photoluminescence spectra were recorded in the 350 to 650 nm wavelength range. A possible cross-relaxation mechanism between the <sup>5</sup>D<sub>3</sub> and the <sup>5</sup>D<sub>4</sub> levels for the concentration quenching of two distinct emission transitions has been described in detail. The dipole–dipole interaction is most responsible for concentration quenching, as evidenced by the Dexter theory. The CIE chromaticity analysis of the Y<sub>2</sub>SiO<sub>5</sub>:Tb<sup>3+</sup> phosphor was illustrated by a CIE 1931 color calculator. These findings demonstrate the suitability of the Tb<sup>3+</sup>-activated Y<sub>2</sub>SiO<sub>5</sub> matrix as a UV-excitable, color-tunable emitter with Tb<sup>3+</sup> ion variations and an efficient green light-emitting phosphor in the fields of solid-state lighting devices.

**Keywords** Y<sub>2</sub>SiO<sub>5</sub> · photoluminescence · Tb<sup>3+</sup> ions · sol–gel

## Introduction

Luminescent phosphors have been extensively studied for their use as color-emitting components in the lighting industry, such as displays, plasma display panels, solid-state lighting, electroluminescent panels, light emitting diodes (LEDs), and scintillator panels for x-ray radiography.<sup>1–4</sup> To meet technological requirements, the materials should be characterized by long periods of work with high transparency and brightness. Therefore, within this framework, finding novel functional materials is a challenging task for

researchers who have turned their attention to inorganic luminescent materials. Several crystal hosts doped with rare-earth elements, such as aluminate garnet (Y<sub>3</sub>Al<sub>5</sub>O<sub>12</sub>), alkaline orthophosphates, and oxyorthosilicates (such as Re<sub>2</sub>SiO<sub>5</sub>) have shown good luminescence properties.<sup>5–7</sup> In this paper, the authors focus on Tb<sup>3+</sup>-doped yttrium oxyorthosilicate (Y<sub>2</sub>SiO<sub>5</sub>) host matrix. Generally, the Y<sub>2</sub>SiO<sub>5</sub> host is known to be an excellent cathodoluminescent phosphor due to its unique physicochemical characteristics, such as efficient chemical and thermal stability with the large stopping potential of the absorption coefficient.<sup>8,9</sup> The persistence of crystalline Y<sub>2</sub>SiO<sub>5</sub> monoclinic phases of X1 or X2 type is visible in the preparation of materials depending on the temperature, and, usually, at a higher temperature (≥ 1300°C), the X2 crystalline phase can be observed.<sup>10,11</sup>

The development of Tb<sup>3+</sup>-doped phosphor stands as a cornerstone in the realm of luminescent materials, heralding advances in various technological domains. These phosphors, comprised of terbium ions integrated into host matrices, exhibit unique photoluminescent properties, making them indispensable in diverse applications.<sup>3</sup> The journey of these phosphors traces back to their inception, when

✉ Vijay Singh  
vijayjiin2006@yahoo.com

<sup>1</sup> Department of Chemical Engineering, Konkuk University, Seoul 05029, Republic of Korea

<sup>2</sup> Department of Physics, Koneru Lakshmaiah Education Foundation, Hyderabad, Telangana 500043, India

<sup>3</sup> Department of Physics, Institute of Aeronautical Engineering (IARE), Hyderabad, Telangana 500043, India

<sup>4</sup> Department of Physics, R.T.M. Nagpur University, Nagpur 440033, India

researchers endeavored to harness the distinctive emission characteristics of Tb<sup>3+</sup> ions to create efficient light-emitting materials.<sup>9</sup> The inception of Tb<sup>3+</sup>-doped phosphors stemmed from the quest to harness the unique luminescence properties of terbium ions within a host matrix. Researchers aimed to exploit the characteristic emission spectrum of Tb<sup>3+</sup> ions, which emits intense and well-defined green light upon excitation by external energy sources.<sup>3,9,11</sup> This distinctive luminescence property, coupled with the ability to manipulate its emission wavelengths and intensity, sparked immense interest in the scientific community. The early stages of development witnessed pioneering efforts in synthesizing and characterizing these phosphors, laying the groundwork for subsequent breakthroughs. Fundamental research into crystal structures, doping concentrations, and fabrication methodologies paved the way for enhanced understanding and control over the luminescence behavior of Tb<sup>3+</sup>-doped phosphors. As technological demands evolved, so did the pursuit of optimizing these materials for a myriad of applications. The continual refinement of synthesis techniques, from traditional powder-based formulations to cutting-edge nanostructured designs, has been instrumental in achieving superior efficiency, stability, and tailored functionalities. The ongoing development and advancement of Tb<sup>3+</sup>-doped phosphors underscore the relentless pursuit of efficiency, reliability, and versatility in luminescent materials.<sup>12</sup> This journey of innovation not only reshapes the landscape of technological applications but also continues to inspire further exploration, promising new frontiers in the realm of luminescence and materials science.

Nevertheless, trivalent terbium (Tb<sup>3+</sup>) ions have emissions in the green region with numerous host materials as described in the local crystal environment.<sup>12,13</sup> Properly excited, they typically exhibit emissions at ~ 489 nm, ~ 540 nm, ~ 580 nm, and ~ 620 nm, which can be attributed to <sup>5</sup>D<sub>4</sub> → <sup>7</sup>F<sub>6</sub>, <sup>7</sup>F<sub>5</sub>, <sup>7</sup>F<sub>4</sub>, and <sup>7</sup>F<sub>3</sub> transitions, respectively.<sup>14</sup> While the narrow emission band was attributed to the spin-forbidden *4f-4f* transitions, the intense emission of the <sup>5</sup>D<sub>4</sub> → <sup>7</sup>F<sub>5</sub> electronic transition is the prime contributor to the phosphor's green emission. The high emission band that leads to spin-allowed transitions is unsuitable for LEDs, hindering the application of most Tb<sup>3+</sup>-based host phosphors for w-LEDs development despite its optimal green luminescence.<sup>15-17</sup> This has motivated thorough research into the development of Tb<sup>3+</sup> ions as luminescent phosphors for green light emission for application in various fields, including mercury-excited lamps and display devices. Orthosilicate-based luminescent phosphor materials are generally environmentally friendly as they do not contain toxic materials like sulfur.<sup>18</sup> Various inorganic luminescent materials composed of rare-earth-activated oxyorthosilicates have been widely described, including Y<sub>2</sub>SiO<sub>5</sub>:Tb<sup>3+</sup>, Eu<sup>3+</sup>,<sup>19</sup> Y<sub>2</sub>SiO<sub>5</sub>:Tb<sup>3+</sup>,<sup>20</sup> X<sub>2</sub>-Y<sub>2</sub>SiO<sub>5</sub>:Tb<sup>3+</sup>,<sup>21</sup> Tb-doped Y<sub>2</sub>SiO<sub>5</sub>,<sup>22</sup> and

Y<sub>2</sub>SiO<sub>5</sub>:Ce.<sup>23</sup> Oxide phosphors have been synthesized using various methods, such as solid-state reaction,<sup>24</sup> spray pyrolysis,<sup>25</sup> combustion synthesis,<sup>26</sup> solid-liquid reaction,<sup>27</sup> and co-precipitation,<sup>21</sup> respectively.

It has recently been noticed that Tb<sup>3+</sup>-activated phosphors exhibit tunable blue-to-green emissions due to luminescence quenching, which are associated with the cross-relaxation mechanism between the two excited levels, <sup>5</sup>D<sub>3</sub> and <sup>5</sup>D<sub>4</sub> of Tb<sup>3+</sup> ions, occurring in the host crystal lattices and activator concentration.<sup>28-30</sup> Kang et al.,<sup>31</sup> Li et al.,<sup>32</sup> and Zang et al.<sup>33</sup> investigated and then concluded that the crystal structure of X2 presents better photoluminescence characteristics than the X1-type in Tb<sup>3+</sup>:Y<sub>2</sub>SiO<sub>5</sub> phosphor. Afandi et al.<sup>34</sup> prepared an X2-type crystal structure of Tb<sup>3+</sup>:Y<sub>2</sub>SiO<sub>5</sub> phosphors at high temperatures through solid-state reaction. They observed tunable emissions with a variation of Tb<sup>3+</sup> ions, typically blue in color with 0.1% of Tb<sup>3+</sup> ions and green in color with 1% of Tb<sup>3+</sup> ions, and concluded that phosphor particles with an X2-type crystal structure in Tb<sup>3+</sup>:Y<sub>2</sub>SiO<sub>5</sub> phosphors are useful for the development of display technology.

In this paper, the structural and luminescence properties of Tb<sup>3+</sup>-activated Y<sub>2</sub>SiO<sub>5</sub> phosphor samples were studied in order to observe tunable emissions with the doping of Tb<sup>3+</sup> ions concentrations over a wide range from 1 mol% to 11 mol%. Structural and functional group characteristics were investigated by x-ray diffraction (XRD) and Fourier-transform infrared (FT-IR) spectroscopy. The photoluminescence properties and CIE (Commission International de L'Eclairage) coordinates of the prepared Tb<sup>3+</sup>:Y<sub>2</sub>SiO<sub>5</sub> phosphor have been examined in detail. The novelty of the obtained results lies in the ability to achieve tunable emissions of blue-green by altering the Tb<sup>3+</sup> ion concentration in the X1-type crystallite structure of Tb<sup>3+</sup>:Y<sub>2</sub>SiO<sub>5</sub> phosphors which is now limited to X2-type only. To summarize our investigation, the Tb<sup>3+</sup>:Y<sub>2</sub>SiO<sub>5</sub> exhibited outstanding photoluminescence characteristics that support its promising potential as a blue-green color-emitting phosphor material for displays.

## Experimental

A series of Y<sub>2</sub>SiO<sub>5</sub>:xTb<sup>3+</sup> (*x* = 0.01 mol, 0.03 mol, 0.05 mol, 0.07 mol, 0.09 mol, 0.11 mol) luminescent samples were prepared using the sol-gel method. Stoichiometric amounts of the starting materials Y(NO<sub>3</sub>)<sub>3</sub>·6H<sub>2</sub>O, SiO<sub>2</sub>, Tb(NO<sub>3</sub>)<sub>3</sub>·xH<sub>2</sub>O, and citric acid (the molar ratio of metal ion to citric acid was 1:2) were used for the synthesis process. The compounds were accurately weighed and then added to a 0.05-L glass beaker containing 0.012 L of deionized water. The resulting solution was thoroughly mixed with a magnetic stirrer for over 1 h at room

temperature. The homogeneous mixture was initially inserted into an oven to obtain the dry gel. The dried gels were heated at 400°C for 20 min, then crushed, and finally sintered at 1100°C for 3 h. The entire sintering procedure of the prepared sample was performed in the air. The block diagram of the synthesis process is depicted in Fig. 1.

The samples' phase identification was conducted by analyzing their XRD patterns using a RIGAKU (Miniflex-II) diffractometer in the  $2\theta$  range of 12–60 degrees. Diffraction patterns were examined at a scan rate of 0.08/s with a scanning angular range of 10°–60°. A Thermo Fisher Nicolet (6700) FT-IR spectrometer was used to detect the various structural groups present in the samples. Photoluminescence

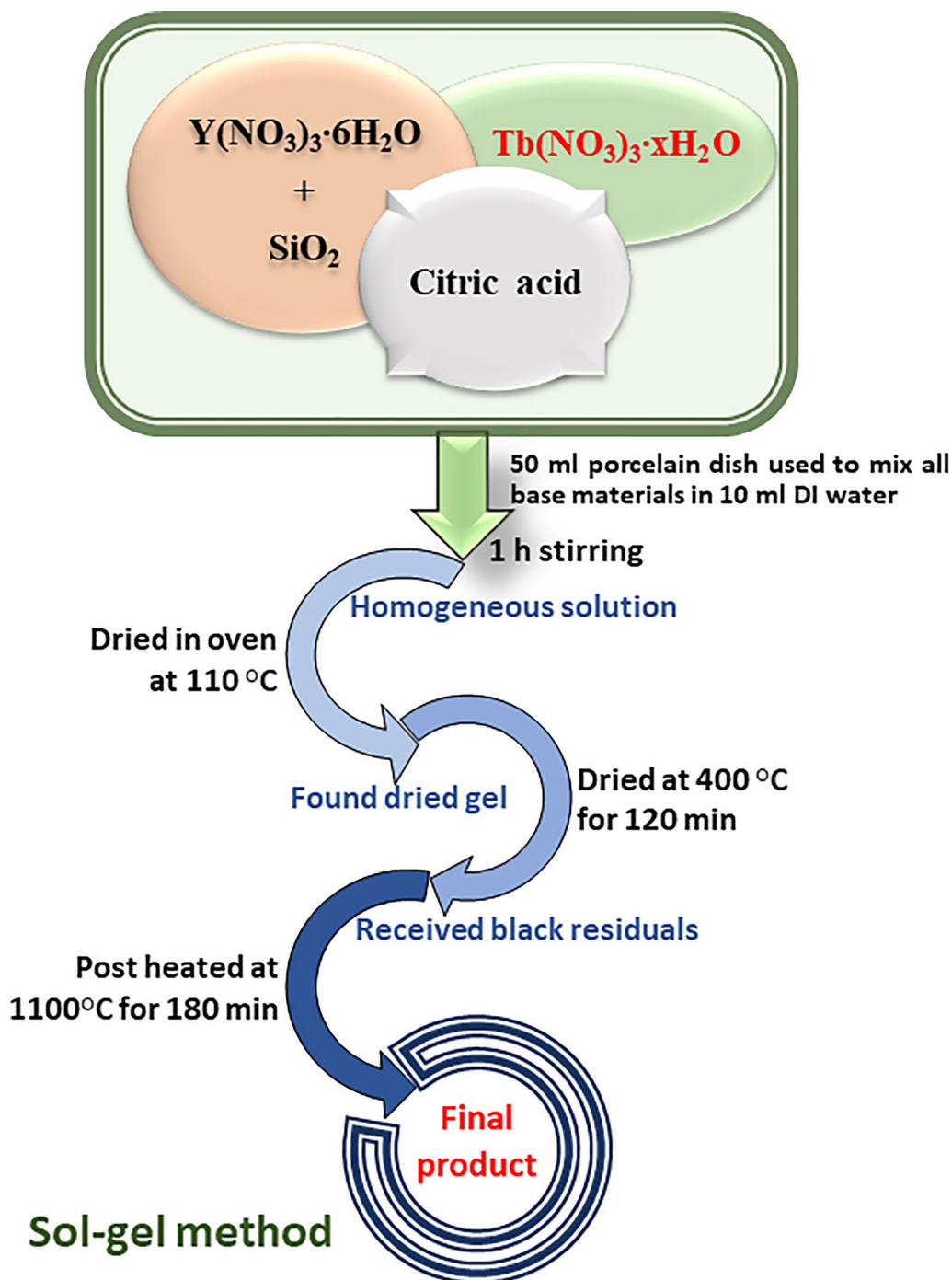
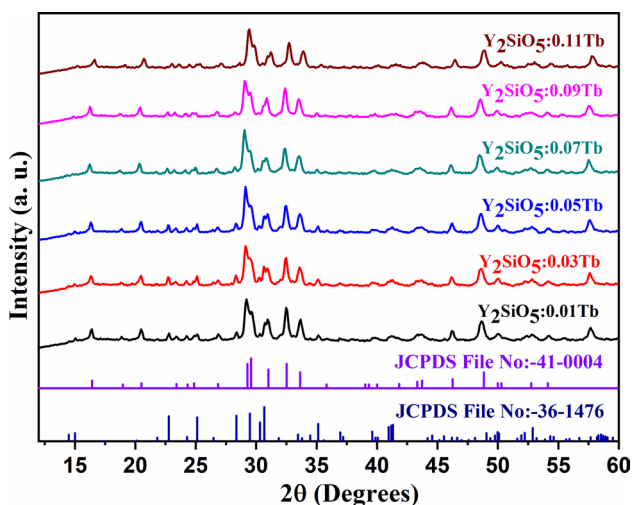


Fig. 1 Flow chart of the synthesis method.

characterization was performed with RF-5301PC spectrofluorophotometer (Shimadzu, Japan).

## Results and Discussion

According to previous works on Tb<sup>3+</sup>:Y<sub>2</sub>SiO<sub>5</sub> phosphor matrices, the crystal lattice distortion or phase transition can occur at the synthesis temperature, although Y<sup>3+</sup> and Tb<sup>3+</sup> ionic radii are almost equal. It is known that phase purity is determined by evaluating XRD data. Figure 2 shows the XRD pattern of the prepared Tb<sup>3+</sup>:Y<sub>2</sub>SiO<sub>5</sub> phosphor samples. All the diffraction peaks were observed to be indexed with the low-temperature monoclinic phase Y<sub>2</sub>SiO<sub>5</sub> (41-0004, JCPDS file) with a space group of P21/c and the high-temperature monoclinic phase Y<sub>2</sub>SiO<sub>5</sub> (36-1476, JCPDS file) with a space symmetry of *I*\**a*.<sup>35,36</sup> It is interesting to note that increasing the concentration of Tb<sup>3+</sup> in the Y<sub>2</sub>SiO<sub>5</sub> host matrix does not induce any distortions in the space group and that the major planes correspond to the low-temperature phase of Y<sub>2</sub>SiO<sub>5</sub>. Therefore, we achieved a stable and homogeneous crystal plane and a uniform increase in the concentration of Tb<sup>3+</sup> ions (1–11 mol%) during the synthesis of the samples at 1100 °C by the sol–gel method. These results suggest that the observed crystal phase is of the X1 type for all the series of samples, and thus the sol–gel synthesis offers excellent intercalation of elements in the starting materials and high cation homogeneity, which lowers the diffusion resistance. The low-temperature phase of Y<sub>2</sub>SiO<sub>5</sub> plays a crucial role in influencing the structural and optical properties of the synthesized Tb<sup>3+</sup>:Y<sub>2</sub>SiO<sub>5</sub> phosphor. The choice of a lower synthesis temperature, in comparison to higher-temperature phases, is intentional and designed



**Fig. 2** Powder XRD patterns of Y<sub>2</sub>SiO<sub>5</sub>:xTb<sup>3+</sup> (0.01 ≤ x ≤ 0.11) phosphors.

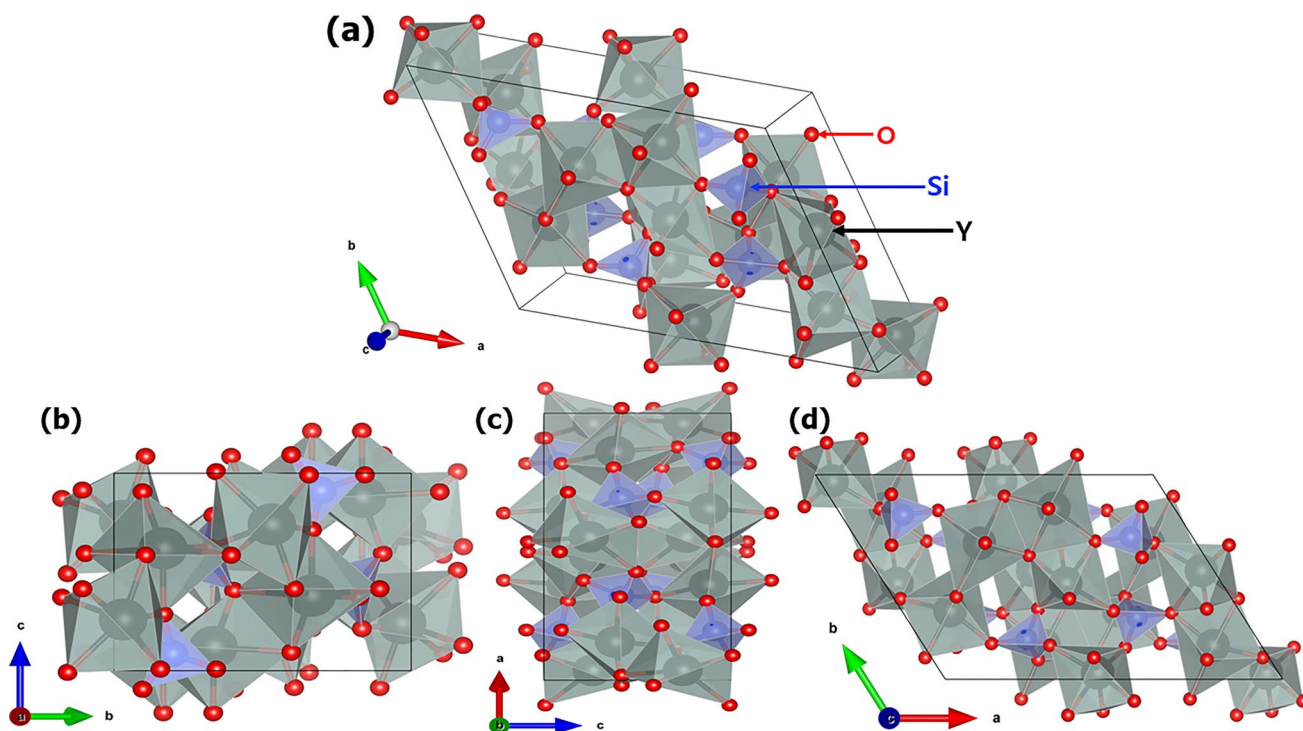
to favor the formation of a specific crystal structure. Low-temperature phases often exhibit distinct crystallographic arrangements, and, in our case, it contributes to achieving the desired structural characteristics in Y<sub>2</sub>SiO<sub>5</sub>.

Figure 3 depicts the crystal structure of the Y<sub>2</sub>SiO<sub>5</sub> host material by using the VESTA software. The CIF file number –1001838 was obtained directly from open crystallographic data.<sup>37,38</sup> The crystal structure parameters of the yttrium oxyorthosilicate (Y<sub>2</sub>SiO<sub>5</sub>) phosphor are ( $\alpha, \beta = 90, \gamma = 122.25$ ), ( $a = 14.58320 \text{ \AA}, b = 10.5120 \text{ \AA}, c = 6.8152 \text{ \AA}$ ) and the cell volume,  $V = 884.2910 \text{ \AA}^3$ . The resulting X1-type crystal phase structure of the Tb<sup>3+</sup>:Y<sub>2</sub>SiO<sub>5</sub> phosphor was monoclinic with P21/c and the local symmetry consisted of two distinct Y<sup>3+</sup> sites: (1) 9-coordinated with 8 Si-O bonded atoms and 1 without silicon-bonded atom (free oxygen (O) atoms); and (2) 7-coordinated with 4 Si-O bonded atoms and 3 free O atoms. Due to the equal ionic radii of Tb<sup>3+</sup> and Y<sup>3+</sup>, Tb<sup>3+</sup> ions can be expected to be situated at local Y<sup>3+</sup> sites. The percentage difference in radius between the active ion (Tb<sup>3+</sup>) and the host cation (Y<sup>3+</sup>) can be determined by<sup>39</sup>:

$$\delta_r = \frac{R_{Tb}(\text{CN}) - R_Y(\text{CN})}{R_{Tb}(\text{CN})} \times 100 \quad (1)$$

where  $\delta_r$  is the percentage difference in the radii, CN is the coordination number, and  $R_{Tb}$  and  $R_Y$  are the radii of the active ion and the host cation, respectively.  $R_{Tb}$  and  $R_Y$  with coordination number 6 are 0.92 Å and 0.9 Å. The estimated  $\delta_r$  is ~ 2.2, which is an excellent acceptable range for effective ionic substitution ( $\leq 3\%$ ).<sup>40</sup>

Figure 4 shows the FI-IR spectra of Tb<sup>3+</sup>:Y<sub>2</sub>SiO<sub>5</sub> phosphors. The band between 4000 cm<sup>-1</sup> to 3500 cm<sup>-1</sup> is related to the stretching mode of O-H molecules. The band at 1528 cm<sup>-1</sup> is attributed to the C=C bond stretching those results from the alkoxy groups. The Y(NO<sub>3</sub>)<sub>3</sub> absorption bands exhibited vibration peaks of the NO<sub>3</sub> group at ~ 1029 cm<sup>-1</sup>, ~ 933 cm<sup>-1</sup>, and ~ 885 cm<sup>-1</sup>, which are associated with the *m*(NO<sub>2</sub>), *m*(NO) and *m*(NO<sub>3</sub>) bands, respectively.<sup>41,42</sup> This confirms the existence of these ions in the gels. The peak at 698 cm<sup>-1</sup> corresponds to the stretching vibrations of the Si-O-Si bonds within the Y<sub>2</sub>SiO<sub>5</sub> crystal lattice. This frequency is typically associated with the symmetric stretching mode of the Si-O-Si unit in the structure.<sup>43</sup> The peak at approximately 2354 cm<sup>-1</sup> could correspond to a variety of possibilities depending on the specific environment of the material. It could potentially indicate the presence of C-H stretching vibrations if there are any organic contaminants or residual carbon-based compounds present. The sample exhibited a Y-O bond absorption band appearing at ~ 555 cm<sup>-1</sup>. The FT-IR spectrum of Y<sub>2</sub>SiO<sub>5</sub> shows a weaker peak at 492 cm<sup>-1</sup>, which corresponds to the Si-O bending modes.



**Fig. 3** Crystal structure of  $Y_2SiO_5$  (a) standard orientation, (b, c, and d) three different orientations, 100, 010, and 001, respectively.

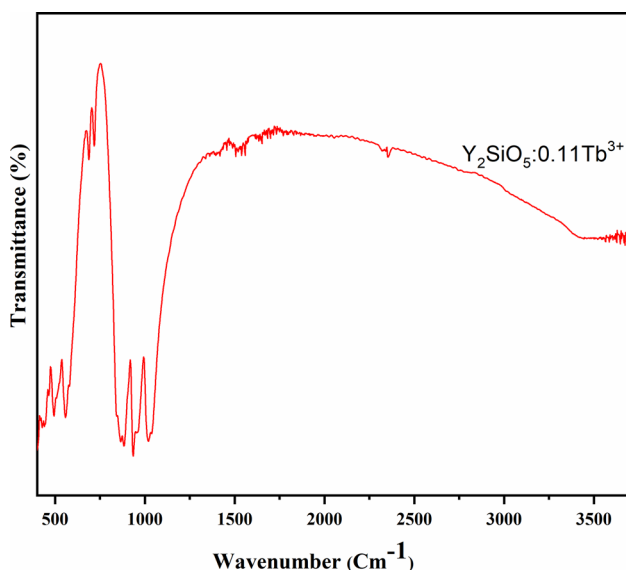


**Fig. 4** FT-IR spectrum of  $Y_2SiO_5:0.11Tb^{3+}$  phosphor.

Figure 5 shows the photoluminescence excitation and emission spectra of  $Tb^{3+}:Y_2SiO_5$  phosphors. Photoluminescence excitation spectra are recorded in the 220–400 nm wavelength range by monitoring the emission at 543 nm ( $Tb^{3+}: ^5D_4 \rightarrow ^7F_5$ ), shown in Fig. 5a. Two significant wide bands were discovered in the ultraviolet spectral region. The

bands at 244 nm and 302 nm would be attributed to the mixing of a charge–transfer band due to Tb–O interaction and the  $4f$ – $5d$  transition bands in the  $Tb^{3+}$  center. The several other small peaks in the range of 300–400 nm represent the  $f$ – $f$  transition of  $Tb^{3+}$ .<sup>44</sup> It can be seen that the excitation band with an intensity of 302 nm changes with the concentration's variation, whereas a clear increase in the intensity of the 244-nm peak was observed. In this context, we assume that the  $Tb^{3+}$  ions are in an octahedral environment because they excited  $Tb^{3+}$  levels of the  $4f^75d^1$  configuration in the  $Tb^{3+}$  centers.<sup>45</sup> The yttrium sites in the  $Y_2SiO_5$  host lattice are 7 and 9 coordinated with oxides (P21/c symmetry group), which restricts the crystal field splitting of the current system to octahedral crystal field-splitting approximations.<sup>46,47</sup> However, the crystal field splitting helps to understand the excitation of  $Tb^{3+}:Y_2SiO_5$ . Given the spin selection rules, a weak intense peak has a weak oscillator strength originating from a spin-forbidden, and a strong intense peak has a strong oscillator strength coming from a spin-allowed. The excitation peak at 244 nm was most appropriate for the excellent emissions from the prepared phosphor.

The photoluminescence spectra of the  $Tb^{3+}:Y_2SiO_5$  phosphors were measured in the wavelength range of 350–650 nm upon a 244-nm exciter and are depicted in Fig. 5b. The observed emission peaks are associated with the transitions originating from the  $^5D_3$  and  $^5D_4$  levels to the lower  $^7F_j$  levels. The electronic transitions  $^5D_3 \rightarrow ^7F_6$ ,

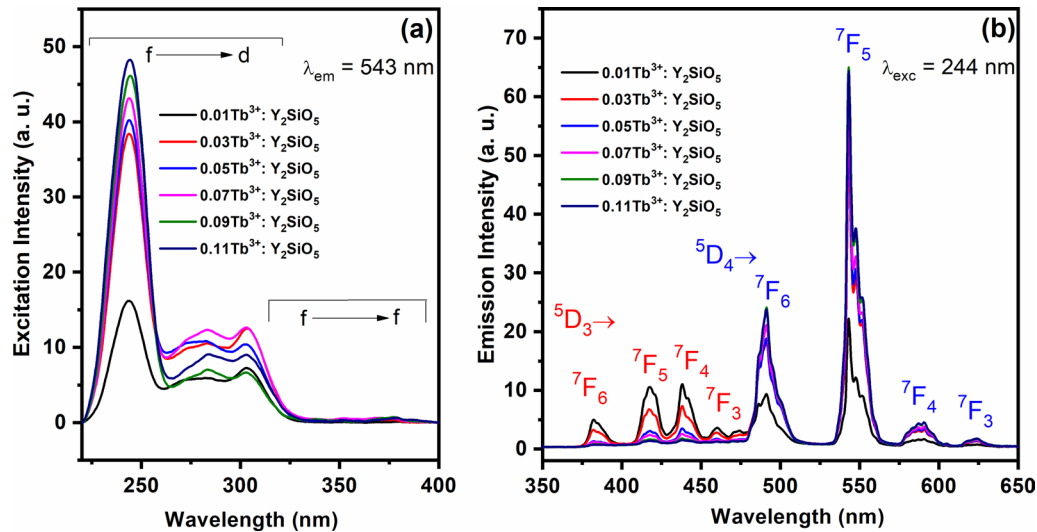


**Fig. 5** (a) Excitation ( $\lambda_{em} = 543$  nm) and (b) photoluminescence spectra ( $\lambda_{exc} = 244$  nm) of Y<sub>2</sub>SiO<sub>5</sub>:xTb<sup>3+</sup> ( $0.01 \leq x \leq 0.11$ ) phosphors.

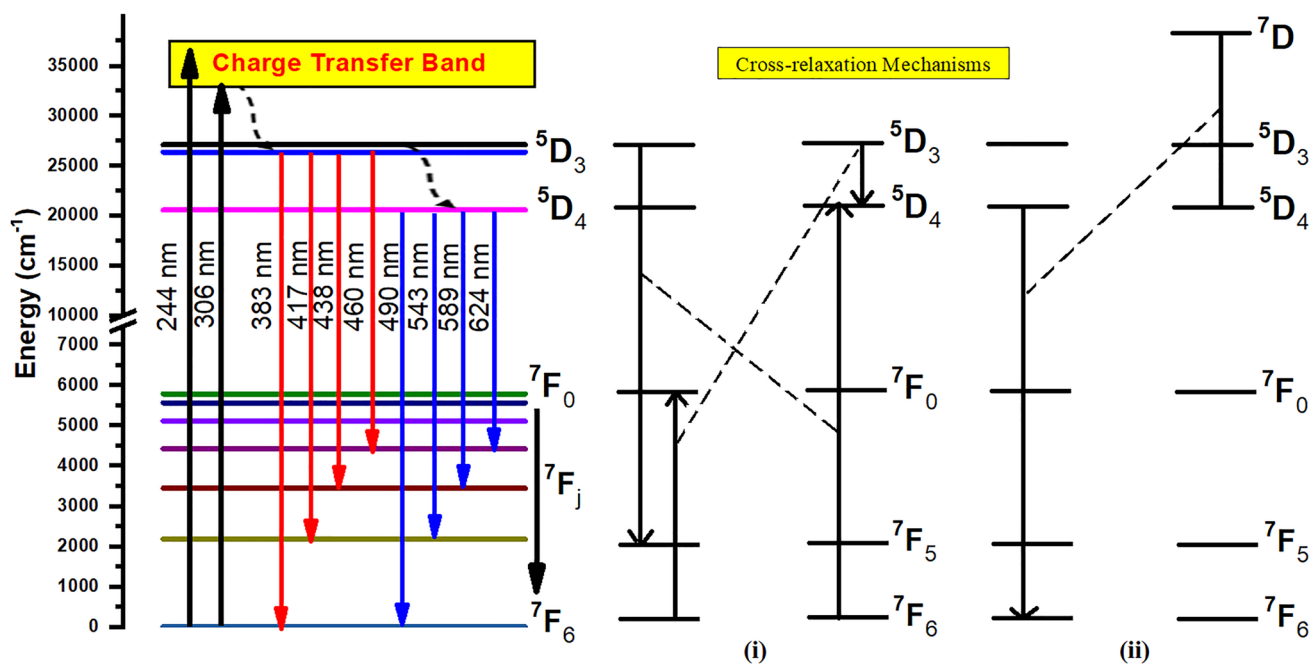
<sup>7</sup>F<sub>5</sub>, <sup>7</sup>F<sub>4</sub> and <sup>7</sup>F<sub>3</sub> correspond to the emission peak centers at ~ 383 nm, ~ 417 nm, ~ 438 nm and ~ 460 nm, respectively, and <sup>5</sup>D<sub>4</sub> → <sup>7</sup>F<sub>6</sub>, <sup>7</sup>F<sub>5</sub>, <sup>7</sup>F<sub>4</sub>, and <sup>7</sup>F<sub>3</sub> transitions are corresponding to the peak centers at ~ 490 nm, ~ 543 nm, ~ 589 nm and ~ 624 nm, respectively. These two distinct <sup>5</sup>D<sub>J</sub> levels originating transitions are created by the splitting effect of the crystal field. Moreover, the <sup>5</sup>D<sub>4</sub> → <sup>7</sup>F<sub>6</sub> transition in blue light emission was attributed to the electric dipole transition described by the local environment of the crystal field. The band at ~ 543 nm is the symmetry of the crystal field-dependent one, whereas the <sup>5</sup>D<sub>4</sub> → <sup>7</sup>F<sub>5</sub> located in the green light emission region corresponds to the magnetic dipole transition and is free from the crystal field strength.<sup>44</sup> The decrease in the emission intensity of transitions occurring from higher energy states in Tb-doped Y<sub>2</sub>SiO<sub>5</sub> can be influenced by several factors. As the energy levels increase, there is a higher probability of non-radiative decay pathways becoming more dominant. Non-radiative processes, such as phonon-assisted relaxation or energy transfer to defects or impurities within the crystal lattice, can reduce the efficiency of radiative emissions from higher energy states. These non-radiative pathways compete with the radiative transitions, leading to a decrease in the observed emission intensity. In complex materials like Y<sub>2</sub>SiO<sub>5</sub>, the crystal field around the Tb ions can lead to Stark splitting, causing the energy levels to separate. Transitions originating from higher Stark levels might have lower probabilities of radiative emission due to their altered energy landscapes, contributing to reduced emission intensity. Figure 6 shows an energy-level schematic of the excitation and emission mechanism of Tb<sup>3+</sup>:Y<sub>2</sub>SiO<sub>5</sub> phosphors (cross-relaxation mechanisms, non-radiative transition).

Figure 7 shows the concentration-quenching behavior of the strong emission transitions associated with both the <sup>5</sup>D<sub>3</sub> and <sup>5</sup>D<sub>4</sub> levels to the <sup>7</sup>F<sub>J</sub> ( $J = 4, 5$  &  $6$ ) levels as the Tb<sup>3+</sup> concentration increases. It can be seen that the maximum emission intensity of the <sup>5</sup>D<sub>3</sub> → <sup>7</sup>F<sub>5</sub>, <sup>7</sup>F<sub>4</sub>, and <sup>5</sup>D<sub>4</sub> → <sup>7</sup>F<sub>6</sub>, <sup>7</sup>F<sub>5</sub> transitions was obtained for 1 mol% and 9 mol% of Tb<sup>3+</sup> ions in Tb<sup>3+</sup>:Y<sub>2</sub>SiO<sub>5</sub> phosphors. The observed concentration quenching is caused by a non-radiative transition from <sup>5</sup>D<sub>3</sub> to <sup>5</sup>D<sub>4</sub> levels through a cross-relaxation mechanism. The concentration quenching observed ranged from approximately 1 mol% to 9 mol% of Tb<sup>3+</sup> ions for the <sup>5</sup>D<sub>3</sub> and <sup>5</sup>D<sub>4</sub> excited levels due to the energy transfer process, multi-ion interaction, and localized crystal field effect. In the <sup>5</sup>D<sub>3</sub> to <sup>5</sup>D<sub>4</sub> cross-relaxation mechanism, in which the energy transfer is possible from Tb<sup>3+</sup>-Tb<sup>3+</sup> ions in single-doped systems, the critical distance between donor and acceptor ions can be estimated using Bassle's equation<sup>48</sup>:

$$R_c = 2 \left[ \frac{3V}{4\pi NX_c} \right]^{1/3} \quad (2)$$

where  $V$  is the cell volume ( $884.2910 \text{ \AA}^3$ ),  $N$  is the availability of four Y<sup>3+</sup> in the unit cell, and  $X_c$  is the critical concentration of Tb<sup>3+</sup> ions. The  $R_c$  for 1 mol% and 9 mol% of Tb<sup>3+</sup> was found to be about  $38.54 \text{ \AA}$  and  $16.39 \text{ \AA}$ , respectively, from the concentration-quenching data from the <sup>5</sup>D<sub>3</sub> → <sup>7</sup>F<sub>5</sub> and <sup>5</sup>D<sub>4</sub> → <sup>7</sup>F<sub>5</sub> emission peaks. The  $R_c$  value from the <sup>5</sup>D<sub>4</sub> → <sup>7</sup>F<sub>5</sub> was more than the <sup>5</sup>D<sub>3</sub> → <sup>7</sup>F<sub>5</sub> for the <sup>5</sup>D<sub>3</sub> → <sup>5</sup>D<sub>4</sub> cross-relaxation, and the  $R_c$  values are much higher than  $5 \text{ \AA}$ , so there is an exchange interaction responsible for the cross-relaxation between <sup>5</sup>D<sub>3</sub> and <sup>5</sup>D<sub>4</sub> levels.

The multipolar interaction mechanism<sup>49</sup> was adopted to provide a more reasonable interpretation of the concentration



**Fig. 6** Partial energy level schematic showing the emission mechanism of Tb<sup>3+</sup> ions under UV light excitations and possible cross-relaxation channels (i and ii) for concentration quenching in Y<sub>2</sub>SiO<sub>5</sub>:Tb<sup>3+</sup> phosphors.

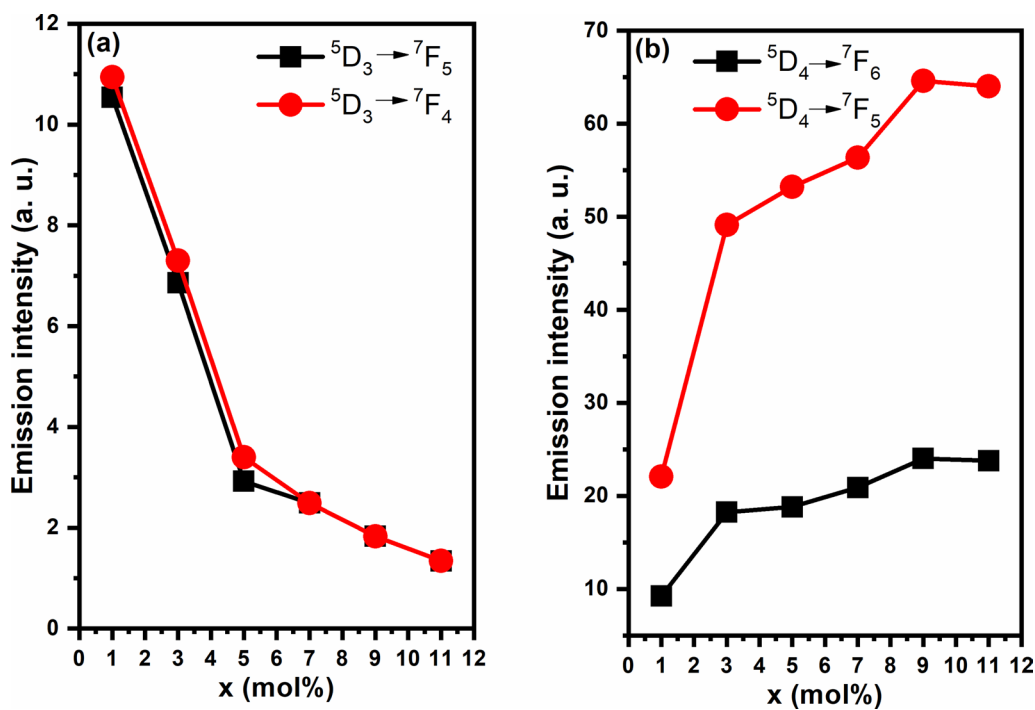


**Fig. 7** Variation of emission intensity as a function of Tb<sup>3+</sup> concentration for the  $^5D_3 \rightarrow ^7F_5$ ,  $^7F_4$ , transitions (a) and the  $^5D_4 \rightarrow ^7F_6$ ,  $^7F_5$  transitions (b) in Y<sub>2</sub>SiO<sub>5</sub>:xTb<sup>3+</sup> phosphors.

quenching of Tb<sup>3+</sup> ions in the Y<sub>2</sub>SiO<sub>5</sub> phosphor. According to Dexter's theory, the exact interaction type between dipole–dipole ( $d \leftrightarrow d$ ), dipole–quadrupole ( $d \leftrightarrow q$ ), and

quadrupole–quadrupole ( $q \leftrightarrow q$ ) interactions for the occurrence of the energy transfer between Tb<sup>3+</sup> ions is obtained by<sup>50,51</sup>:

$$\frac{I}{x} = K \left\{ 1 + \beta(x) \frac{Q}{3} \right\}^{-1} \quad (3)$$

where  $I$  is the intensity of the emission peak,  $x$  is the Tb concentration (1 and 9 mol%), and  $K$  and  $\beta$  are constants.  $Q$  is also a constant for the  $d \leftrightarrow d$  (6),  $d \leftrightarrow q$  (8), and  $q \leftrightarrow q$  (10) interactions. The estimated  $Q$  values in this work are 5.64 and 4.69 for the  $^5D_3 \rightarrow ^7F_5$  and  $^5D_4 \rightarrow ^7F_5$  emission bands, respectively, from the slope value of the linear fit to  $\text{Log}(I/x)$  versus  $\text{Log}(x)$  (see Fig. 8). The  $Q$  value suggests that the specific energy transfer occurs due to dipole–dipole interactions. According to the concentration-quenching luminescence spectral results, two cross-relaxation schemes may be responsible: (1) cross-relaxation from the  $^5D_3$  level to the  $^5D_4$  level, and (2) cross-relaxation from the  $^5D_3$  and/or  $^5D_4$  to the  $^7D$  level (see Fig. 6). Normally, possible quenching may be an energy transfer from the Tb–Tb ion at the  $^5D_3$  level to the  $^5D_4$  levels. One of the Tb ions is excited to the  $^5D_3$  or  $^5D_4$  level with selective excitation and decay to the  $^7F_6$  ground level, then adjacent Tb ions at  $^5D_3$  or  $^5D_4$  level are raised to the  $^7D$  excited state of the  $4f^75d^1$  configuration. Therefore, the luminescence quenching of  $^5D_3 \rightarrow ^7F_5$ ,  $^7F_4$ , and  $^5D_4 \rightarrow ^7F_6$ ,  $^7F_5$  transitions are caused by cross-relaxations (1) and (2), respectively.<sup>49</sup> Among the numerous radiative and non-radiative processes that occur, the leading increase in intensity is noticed for the green emission of the  $^5D_4 \rightarrow ^7F_5$  transition of Tb<sup>3+</sup> ions in Y<sub>2</sub>SiO<sub>5</sub> phosphors.

The CIE chromaticity plot of Y<sub>2</sub>SiO<sub>5</sub>:xTb<sup>3+</sup> phosphors excited at 244 nm is shown in Fig. 9. The CIE coordinates for the Tb<sup>3+</sup>-activated Y<sub>2</sub>SiO<sub>5</sub> phosphors have been determined

since 1931 CIE and are listed in Table I. The variation of the Tb<sup>3+</sup> dopant leads to a shift in the color coordinates of the tunable emission from bluish ( $x = 0.2223$ ,  $y = 0.3072$ ) to green ( $x = 0.2720$ ,  $y = 0.5470$ ). Therefore, the Tb<sup>3+</sup>:Y<sub>2</sub>SiO<sub>5</sub> phosphor is a potential color-adjustable phosphor candidate for UV-based wLEDs. The color purity of the Y<sub>2</sub>SiO<sub>5</sub>:xTb<sup>3+</sup> phosphor was evaluated.<sup>52</sup>

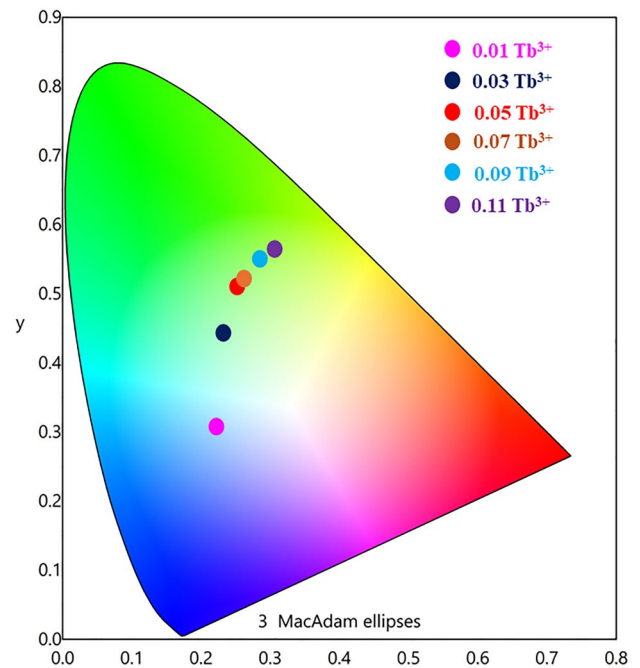


Fig. 9 CIE chromaticity diagram for Y<sub>2</sub>SiO<sub>5</sub>:xTb<sup>3+</sup> phosphors.

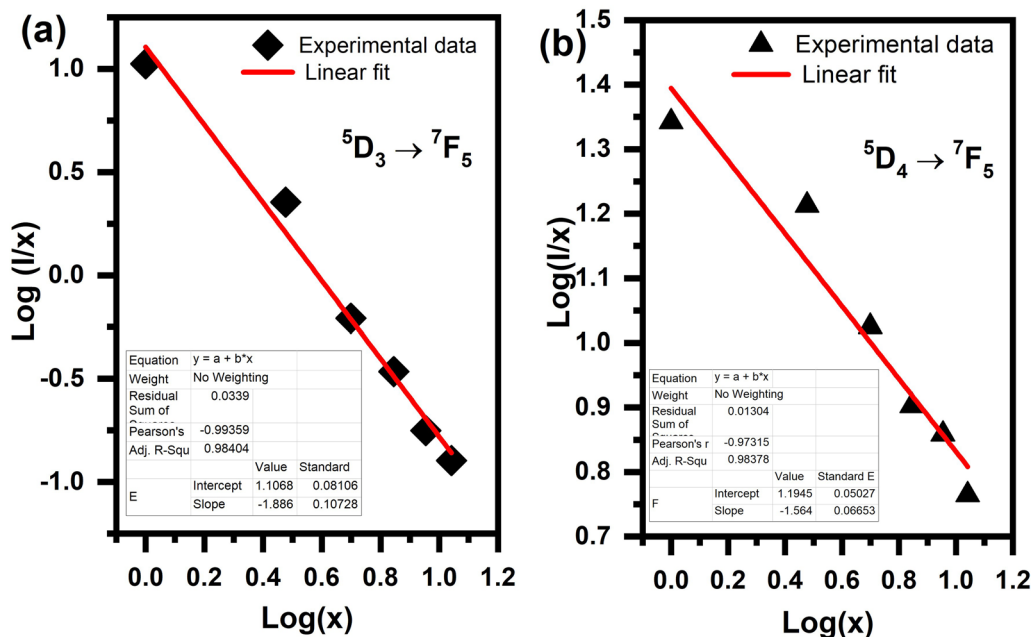


Fig. 8 Plots of  $\text{Log}(I/x)$  versus  $\text{Log}(x)$  for (a)  $^5D_3 \rightarrow ^7F_5$  and (b)  $^5D_4 \rightarrow ^7F_5$  emission transitions in Y<sub>2</sub>SiO<sub>5</sub>:Tb<sup>3+</sup> phosphors.



$$\text{Color purity (\%)} = \frac{\sqrt{(x - x_i)^2 + (y - y_i)^2}}{\sqrt{(x_d - x_i)^2 + (y_d - y_i)^2}} \times 100$$

The CIE color purity for the 0.09 and 0.11 mol concentrations of  $\text{Tb}^{3+}$  in  $\text{Y}_2\text{SiO}_5$  phosphor indicates the suitability of the prepared phosphor for applications in UV excitable solid-state lighting. The color purity of the  $\text{Y}_2\text{SiO}_5$  phosphor doped with a higher concentration of  $\text{Tb}^{3+}$  is approximately 60.96%. The observed lower color purity in the emitted light can be influenced by several factors. The presence of impurities, defects, or variations in the host lattice could lead to deviations in the emission spectrum, affecting the color purity. Also, energy transfer processes among luminescent centers can contribute to a broadening of the emission spectrum, leading to a lower color purity. Understanding and controlling these energy transfer mechanisms are crucial for

**Table 1** CIE chromaticity for  $\text{Y}_2\text{SiO}_5:x\text{Tb}^{3+}$  phosphors ( $0.01 \leq x \leq 0.11$ ) using PL emission ( $\lambda_{\text{exc}} = 244 \text{ nm}$ )

$\text{Y}_2\text{SiO}_5:x\text{Tb}^{3+}$	$\lambda_{\text{exc}} = 244 \text{ nm}$		Color purity%: (sign)
	x	y	
$x = 0.01$	0.2223	0.3072	64.35 (●)
$x = 0.03$	0.2493	0.4503	55.81 (●)
$x = 0.05$	0.2628	0.5076	56.70 (●)
$x = 0.07$	0.2653	0.5224	58.79 (●)
$x = 0.09$	0.2706	0.5443	60.69 (●)
$x = 0.11$	0.2720	0.5470	60.96 (●)

optimizing color quality. In summary, these results confirm the development potential of new luminescent devices that are appropriate as color-tunable emitting and efficient single components of green phosphors in the lighting industry. Figure 10 shows photographic images of (1)  $\text{Y}_2\text{SiO}_5:0.01\text{Tb}^{3+}$  and (2)  $\text{Y}_2\text{SiO}_5:0.11\text{Tb}^{3+}$  green-emitting sol-gel-synthesized luminescent phosphors. These phosphor images show a whitish color in room light and show a prominent greenish color under UV light (excitation wavelength of 254 nm), demonstrating its suitability for as-sold lighting applications.

## Conclusions

A  $\text{Y}_2\text{SiO}_5:\text{Tb}^{3+}$  phosphor set was efficiently prepared by the sol-gel route. The formation of  $\text{Y}_2\text{SiO}_5$  was examined by XRD. The functional group was confirmed by FT-IR study. Under 244 nm excitation, the phosphor exhibited emission spectrum lines in the 350–650 nm wavelength range. The emission peaks are responsible for the transitions originating from  $^5\text{D}_3$  and  $^5\text{D}_4$  levels to the lower  $^7\text{F}_j$  levels of  $\text{Tb}^{3+}$ . The quenching concentration for 1 mol% and 9 mol% of  $\text{Tb}^{3+}$  ions in  $\text{Tb}^{3+}:\text{Y}_2\text{SiO}_5$  is due to the non-radiative transition from the  $^5\text{D}_3$  to  $^5\text{D}_4$  levels via a cross-relaxation mechanism. The detailed cross-relaxation mechanisms by energy transfer are explained using an energy level diagram of  $\text{Tb}^{3+}$  ions. The chromaticity coordinates of the synthesized  $\text{Tb}^{3+}$  ions in the  $\text{Y}_2\text{SiO}_5$  phosphor were calculated and found to range from a bluish color to a green color in the CIE plot with increasing  $\text{Tb}^{3+}$  ions. The color purity of 0.11 mol of  $\text{Tb}^{3+}$ -doped  $\text{Y}_2\text{SiO}_5$  phosphors is 60.9%. Photoluminescence

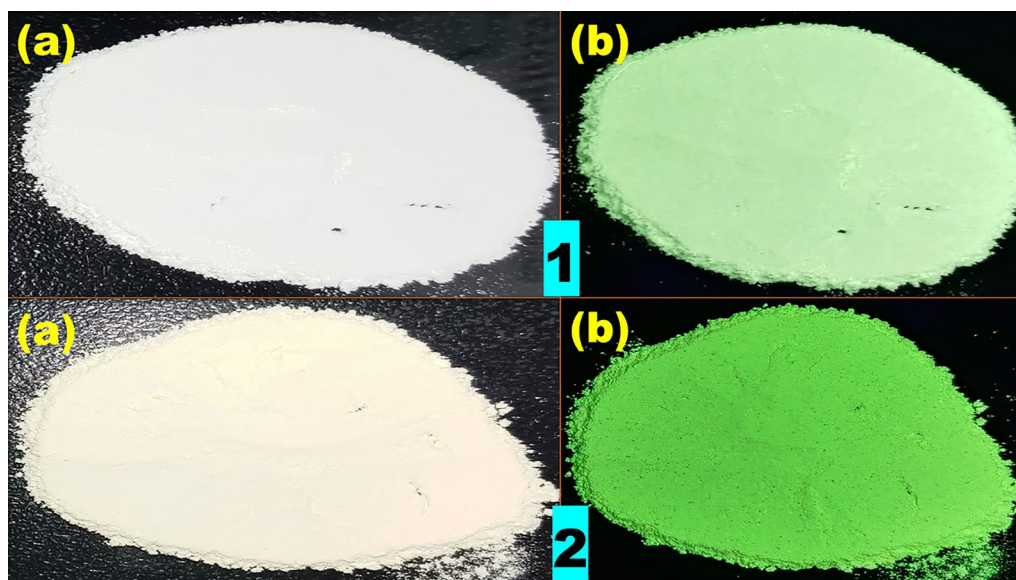


**Fig. 10** Typical photographs of the (1)  $\text{Y}_2\text{SiO}_5:0.01\text{Tb}^{3+}$  and (2)  $\text{Y}_2\text{SiO}_5:0.11\text{Tb}^{3+}$  phosphors: (a) at room light (white powder) and (b) at 254-nm UV light (green powder) (Color figure online).

results suggest that the synthesized Tb<sup>3+</sup>-doped Y<sub>2</sub>SiO<sub>5</sub> phosphor produces tunable color emissions upon UV excitation and an efficient, promising single-green color-emitting phosphor for display device applications.

**Acknowledgment** This work was supported by the National Research Foundation of Korea (NRF) grant funded by the Korea government (MSIT) (No. 2021R1A2C1092509). This paper was supported by the KU Research Professor Program of Konkuk University.

**Conflict of interest** The authors have no conflicts of interest to declare that are relevant to the content of this article.

## References

1. A. Dwivedi, M. Srivastava, A. Srivastava, C. Upadhyay, and S.K. Srivastava, Tunable photoluminescence and energy transfer of Eu<sup>3+</sup>, Ho<sup>3+</sup>-doped Ca<sub>0.05</sub>Y<sub>1.93-x</sub>O<sub>2</sub> nanophosphors for warm white LEDs applications. *Sci. Rep.* 12, 5824 (2022). <https://doi.org/10.1038/s41598-022-09630-x>.
2. Z. Hao, J. Zhang, X. Zhang, X. Sun, Y. Luo, Lu. Shaozhe, and X.-J. Wang, White light emitting diode by using α-Ca<sub>2</sub>P<sub>2</sub>O<sub>7</sub>:Eu<sup>2+</sup>, Mn<sup>2+</sup> phosphor. *Appl. Phys. Lett.* 90, 261113 (2007). <https://doi.org/10.1063/1.2752725>.
3. R. Yantake, M. Kaiheriman, T. Yusufu, and A. Sidike, Effect of Li<sup>+</sup> doping on the luminescence performance of a novel KAlSiO<sub>4</sub>:Tb<sup>3+</sup> green-emitting phosphor. *Sci. Rep.* 11, 5123 (2021). <https://doi.org/10.1038/s41598-021-84220-x>.
4. A. Jain, C.M. Mehare, S. Tamboli, and S.J. Dhoble, Eu<sup>2+</sup>-doped microporous aluminosilicate Ca-chabazite Ca<sub>1.9</sub>Al<sub>3.8</sub>Si<sub>8.2</sub>O<sub>24</sub> phosphor: synthesis and characterization of potential blue phosphor for NUV wLED. *J. Mater. Sci. Mater. Electron.* 32, 6984–6991 (2021). <https://doi.org/10.1007/s10854-021-05406-7>.
5. A. Potdevin, G. Chadeyron, and R. Mahiou, Tb<sup>3+</sup>-doped yttrium garnets: promising tunable green phosphors for solid-state lighting. *Chem. Phys. Lett.* 490, 50–53 (2010). <https://doi.org/10.1016/j.cplett.2010.03.003>.
6. J. Růžička, D. Nižňanský, M. Nikl, R. Kucerková, and C. Cannas, Sol-gel synthesis of cerium-doped yttrium silicates and their luminescent properties. *J. Mater. Res.* 25, 229–234 (2010). <https://doi.org/10.1557/JMR.2010.0039>.
7. C. Cannas, M. Mainas, A. Musinu, G. Piccaluga, S. Enzo, M. Bazzoni, A. Speghini, and M. Bettinelli, Structural investigations and luminescence properties of nanocrystalline europium-doped yttrium silicates prepared by a sol-gel technique. *Opt. Mater.* 29, 585–592 (2007). <https://doi.org/10.1016/j.optmat.2005.11.023>.
8. S. Saha, P.S. Chowdhury, and A. Patra, Luminescence of Ce<sup>3+</sup> in Y<sub>2</sub>SiO<sub>5</sub> nanocrystals: role of crystal structure and crystal size. *J. Phys. Chem. B* 109, 2699–2702 (2005). <https://doi.org/10.1021/jp0462106>.
9. T. Hirai and Y. Kondo, Preparation of Y<sub>2</sub>SiO<sub>5</sub>:Ln<sup>3+</sup> (Ln = Eu, Tb, Sm) and Gd<sub>0.33</sub>(SiO<sub>4</sub>)<sub>6</sub>O<sub>2</sub>:Ln<sup>3+</sup> (Ln = Eu, Tb) phosphor fine particles using an emulsion liquid membrane system. *J. Phys. Chem. C* 111(1), 168–174 (2007). <https://doi.org/10.1021/jp064655j>.
10. H.J. Lee, S.K. Hong, D.S. Jung, S.H. Ju, H.Y. Koo, and Y.C. Kang, The characteristics of X1 type Y<sub>2</sub>SiO<sub>5</sub>: Tb phosphor particles prepared by high-temperature spray pyrolysis. *Ceram. Inter.* 32, 865–870 (2006). <https://doi.org/10.1016/j.ceramint.2005.07.001>.
11. Y.C. Kang, I.W. Lenggoro, K. Okuyama, and S.B. Park, Luminescence characteristics of Y<sub>2</sub>SiO<sub>5</sub>:Tb phosphor particles directly prepared by the spray pyrolysis method. *J. Electrochem. Soc.* 146(3), 1227–1230 (1999). <https://doi.org/10.1149/1.1391750>.
12. R. Naik, S.C. Prashantha, H. Nagabhushana, H.P. Nagaswarupa, K.S. Anantharaju, S.C. Sharma, B.M. Nagabhushana, H.B. Premkumar, and K.M. Girish, Mg<sub>2</sub>SiO<sub>4</sub>:Tb<sup>3+</sup> nanophosphor: Auto ignition route and near UV excited photoluminescence properties for WLEDs. *J. Alloys Compd.* 617, 69–75 (2014). <https://doi.org/10.1016/j.jallcom.2014.07.100>.
13. V.R. Panse, N.S. Kokode, K.N. Shinde, and S.J. Dhoble, Luminescence in microcrystalline green emitting Li<sub>2</sub>Mg<sub>1-x</sub>ZrO<sub>4</sub>:xTb<sup>3+</sup> (0.1 ≤ x ≤ 2.0) phosphor. *Results Phys.* 8, 99–103 (2018). <https://doi.org/10.1016/j.rinp.2017.10.025>.
14. X. Liu, L. Yan, and J. Lin, Synthesis and luminescent properties of LaAlO<sub>3</sub>:RE<sup>3+</sup> (RE = Tm, Tb) nanocrystalline phosphors via a sol-gel process. *J. Phys. Chem. C* 113, 8478–8483 (2009). <https://doi.org/10.1021/jp9013724>.
15. R.K. Tamrakar, and K. Upadhyay, Combustion synthesis and luminescence behaviour of the Tb<sup>3+</sup> doped SrY<sub>2</sub>O<sub>4</sub> phosphor. *J. Electron. Mater.* 47, 651–654 (2018). <https://doi.org/10.1007/s11664-017-5825-x>.
16. J. Zhang, T. Zhao, B. Wang, L. Li, L. Zou, and S. Gan, PEG-assisted hydrothermal synthesis and photoluminescence of CdMoO<sub>4</sub>:Tb<sup>3+</sup> green phosphor. *J. Phys. Chem. Solids* 79, 14–22 (2015). <https://doi.org/10.1016/j.jpcs.2014.11.003>.
17. D.R. Taikar, S. Tamboli, and S.J. Dhoble, Synthesis and photoluminescence properties of red, green and blue emitting LaYO<sub>3</sub>:M (M = Eu<sup>3+</sup>, Tb<sup>3+</sup>, Sm<sup>3+</sup>, Bi<sup>3+</sup>, Pb<sup>2+</sup>) phosphors. *Optik (Stuttg.)* 142, 183–190 (2017). <https://doi.org/10.1016/j.ijleo.2017.05.095>.
18. Y. Kim and S. Park, Preparation and luminescent properties of Eu-substituted barium–yttrium orthosilicate phosphors. *Opt. Mater.* 36, 458–462 (2013). <https://doi.org/10.1016/j.optmat.2013.10.010>.
19. K. Upadhyay, S. Thomas, N. Kalarikkal, and R.K. Tamrakar, Tuning of photoluminescence emission of Y<sub>2</sub>SiO<sub>5</sub>:Tb<sup>3+</sup>, Eu<sup>3+</sup> phosphors by altering the Tb<sup>3+</sup>, Eu<sup>3+</sup> ratio. *Mater. Today Proc.* 34, 484–487 (2018). <https://doi.org/10.1016/j.matpr.2020.03.095>.
20. K.S. Sohn, D.H. Park, J.G. Yoo, and J.S. Kim, Luminescence of pulsed laser deposited Y<sub>2</sub>SiO<sub>5</sub>:Tb<sup>3+</sup> thin film phosphors on flat and corrugated quartz glass substrates. *Japanese J. Appl. Phys., Part 1 Regul. Pap. Short Notes Rev. Pap.* 44, 1787–1791 (2005). <https://doi.org/10.1143/JJAP.44.1787>.
21. Z.H. Zhang, Y.H. Wang, Y. Hao, and W.J. Liu, Synthesis and VUV photoluminescence of green-emitting X<sub>2</sub>-Y<sub>2</sub>SiO<sub>5</sub>:Tb<sup>3+</sup> phosphor for PDP application. *J. Alloys Compd.* 433, 2006–2008 (2007). <https://doi.org/10.1016/j.jallcom.2006.06.087>.
22. D.K. Yim, I.S. Cho, S. Lee, C.H. Kwak, D.H. Kim, J.K. Lee, and K.S. Hong, Synthesis and characteristics of Tb-doped Y<sub>2</sub>SiO<sub>5</sub> nanophosphors and luminescent layer for enhanced photovoltaic cell performance. *J. Nanosci. Nanotechnol.* 11, 8748–8753 (2011). <https://doi.org/10.1166/jnn.2011.3490>.
23. L.E. Muresan, B.F. Oprea, A.I. Cadis, I. Perhaita, and O. Ponta, Studies on Y<sub>2</sub>SiO<sub>5</sub>: Ce phosphors prepared by gel combustion using new fuels. *J. Alloys Compd.* 615, 795–803 (2014). <https://doi.org/10.1016/j.jallcom.2014.07.036>.
24. P. Thiagarajan, B. Tiwari, M. Kottaisamy, N. Rama, and M.S. Ramachandra Rao, UV excitable Y<sub>2-x-y</sub>Gd<sub>y</sub>SiO<sub>5</sub>: Cex phosphors for cool white light emission. *Appl. Phys. A Mater. Sci. Process.* 94, 607–612 (2009). <https://doi.org/10.1007/s00339-008-4861-z>.
25. H.S. Kang, Y.C. Kang, H.D. Park, and Y.G. Shul, Y<sub>2</sub>SiO<sub>5</sub>: Tb phosphor particles prepared from colloidal and aqueous solutions by spray pyrolysis. *Appl. Phys. A Mater. Sci. Process.* 80, 347–351 (2005). <https://doi.org/10.1007/s00339-003-2228-z>.
26. G.S. Maciel and N. Rakov, Thermometric analysis of the near-infrared emission of Nd<sup>3+</sup> in Y<sub>2</sub>SiO<sub>5</sub> ceramic powder prepared by combustion synthesis. *Ceram. Int.* 46, 12165–12171 (2020). <https://doi.org/10.1016/j.ceramint.2020.01.262>.

27. Z. Sun, J. Wang, M. Li, and Y. Zhou, Mechanical properties and damage tolerance of  $Y_2SiO_5$ , *J. Eur. Ceram. Soc.* 28, 2895–2901 (2008). <https://doi.org/10.1016/j.jeurceramsoc.2008.04.029>.
28. J.F.M. dos Santos, I.A.A. Terra, N.G.C. Astrath, F.B. Guimaraes, M.L. Baesso, L.A.O. Nunes, and T. Catunda, Mechanisms of optical losses in the  $^5D_4$  and  $^5D_3$  levels in  $Tb^{3+}$  doped low silica calcium aluminosilicate glasses. *J. Appl. Phys.* 117, 053102 (2015). <https://doi.org/10.1063/1.4906781>.
29. A. Lushchik, C. Lushchik, I. Kudryavtseva, A. Maaros, V. Nagirnyi, and F. Savikhin, Resonant processes causing photon multiplication in  $CaSO_4:Tb^{3+}$ . *Radiat. Meas.* 56, 139–142 (2013). <https://doi.org/10.1016/j.radmeas.2013.01.037>.
30. A.D. Sontakke, K. Biswas, and K. Annapurna, Concentration-dependent luminescence of  $Tb^{3+}$  ions in high calcium aluminosilicate glasses. *J. Lumin.* 129, 1347–1355 (2009). <https://doi.org/10.1016/j.jlumin.2009.06.027>.
31. H. Kang, Y. Kang, H. Park, and Y. Shul, Green-emitting yttrium silicate phosphor particles prepared by large scale ultrasonic spray pyrolysis. *Kor. J. Chem. Eng.* 20, 930–933 (2003). <https://doi.org/10.1007/BF02697301>.
32. X. Li, H. Jiao, X. Wang, Z. Zeng, and X. Jing,  $Y_2SiO_5:Ce^{3+}$  particle growth during sol–gel preparation. *J. Rare Earths* 28, 504–508 (2010). [https://doi.org/10.1016/S1002-0721\(09\)60141-1](https://doi.org/10.1016/S1002-0721(09)60141-1).
33. X. Zhang, L. Zhou, Q. Pang, J. Shi, and M. Gong, Tunable luminescence and  $Ce^{3+} \rightarrow Tb^{3+} \rightarrow Eu^{3+}$  energy transfer of broadband-excited and narrow line red emitting  $Y_2SiO_5:Ce^{3+}, Tb^{3+}, Eu^{3+}$  phosphor. *J. Phys. Chem. C* 118, 7591–7598 (2014). <https://doi.org/10.1021/jp412702g>.
34. M.M. Afandi, G. Antariksa, H. Kang, T. Kang, and J. Kim, Blue-green tunable electroluminescence from  $Y_2SiO_5:Tb^{3+}$  phosphor. *J. Lumin.* 251, 119201 (2022). <https://doi.org/10.1016/j.jlumin.2022.119201>.
35. R.K.T. Kanchan Upadhyay, S. Thomas, and N. Kalarikkal, Effect of synthesis process on particle size and band gap of  $Er^{3+}$  doped  $Y_2SiO_5$ . *AIP Conf. Proc.* 030017, 2–9 (2019). <https://doi.org/10.1063/1.5100444>.
36. D. Meiss, W. Wischert, and S. Kemmler-Sack, Luminescence of the System  $(Y, Gd, Tb)_2SiO_5:Eu^{3+}$ . *Phys. Status Solidi* 133, 575–584 (1992). <https://doi.org/10.1002/pssa.2211330243>.
37. Y. Luo, J. Wang, J. Wang, J. Li, and Z. Hu, Theoretical predictions on elastic stiffness and intrinsic thermal conductivities of yttrium silicates. *J. Am. Ceram. Soc.* 97, 945–951 (2014). <https://doi.org/10.1111/jace.12764>.
38. Z. Tian, C. Lin, L. Zheng, L. Sun, J. Li, and J. Wang, Defect-mediated multiple-enhancement of phonon scattering and decrement of thermal conductivity in  $(Y_xYb_{1-x})_2SiO_5$  solid solution. *Acta Mater.* 144, 292–304 (2018). <https://doi.org/10.1016/j.actamat.2017.10.064>.
39. H. Li, R. Pang, G. Liu, W. Sun, D. Li, L. Jiang, S. Zhang, C. Li, J. Feng, and H. Zhang, synthesis and luminescence properties of  $Bi^{3+}$ -activated  $K_2MgGeO_4$ : a promising high brightness orange-emitting phosphor for WLEDs conversion. *Inorg. Chem.* 57, 12303–12311 (2018). <https://doi.org/10.1021/acs.inorgchem.8b02025>.
40. A.M. Pires and M.R. Davolos, Luminescence of europium (III) and manganese (II) in barium and zinc orthosilicate. *Chem. Mater.* 13, 21–27 (2001). <https://doi.org/10.1021/cm000063g>.
41. J. Li, Y. Pan, F. Qiu, Y. Wu, and J. Guo, Nanostructured Nd:YAG powders via gel combustion: the influence of citrate-to-nitrate ratio. *Ceram. Int.* 34, 141–149 (2008). <https://doi.org/10.1016/j.ceramint.2006.09.002>.
42. S. Esposito, M. Turco, G. Ramis, G. Bagnasco, P. Pernice, C. Pagliuca, M. Bevilacqua, and A. Aronne, Cobalt-silicon mixed oxide nanocomposites by modified sol–gel method. *J. Solid State Chem.* 180, 3341–3350 (2007). <https://doi.org/10.1016/j.jssc.2007.09.032>.
43. D. Boyer and B. Derby, Yttrium silicate powders produced by the sol–gel method, structural and thermal characterization. *J. Am. Ceram. Soc.* 86, 1595–1597 (2003). <https://doi.org/10.1111/j.1151-2916.2003.tb03520.x>.
44. Z. Liu, X. Sun, S. Xu, J. Lian, X. Li, Z. Xiu, Q. Li, D. Huo, and J.G. Li,  $Tb^{3+}$ - and  $Eu^{3+}$ -doped lanthanum oxysulfide nanocrystals. Gelatin-templated synthesis and luminescence properties. *J. Phys. Chem. C* 112, 2353–2358 (2008). <https://doi.org/10.1021/jp0764687>.
45. R.E. Newnham, M.J. Redman, and R.P. Santoro, Crystal structure of yttrium and other rare earth borates. *J. Am. Ceram. Soc.* 46, 253 (1963). <https://doi.org/10.1111/j.1151-2916.1963.tb11721.x>.
46. J. Felsche, The crystal chemistry of rare earth silicates. *Struct. Bonding* 13, 99 (1973). [https://doi.org/10.1007/3-540-06125-8\\_3](https://doi.org/10.1007/3-540-06125-8_3).
47. P. Ghosh, S. Sadhu, and A. Patra, Preparation and photoluminescence properties of  $Y_2SiO_5:Eu^{3+}$  nanocrystals. *Phys. Chem. Chem. Phys.* 8, 3342–3348 (2006). <https://doi.org/10.1039/B603273G>.
48. M. MangalaGowri, R.B. Basavaraj, and H. Nagabhushana, Sonochemical synthesis of dual phase  $Y_2SiO_5:Eu^{3+}$  nanopowder: luminescence and Judd–Ofelt analysis. *Inter. J. Lumin. Appl.* 19, 594–603 (2019).
49. Y.Y. Choi, K.S. Sohn, H.D. Park, and S.Y. Choi, Luminescence and decay behaviors of Tb-doped yttrium silicate. *J. Mater. Res.* 16(3), 881–889 (2001). <https://doi.org/10.1557/JMR.2001.0116>.
50. Y. Kumar, M. Pal, M. Herrera, and X. Mathew, Effect of Eu ion incorporation on the emission behavior of  $Y_2O_3$  nanophosphors: a detailed study of structural and optical properties. *Opt. Mater.* 60, 159–168 (2016). <https://doi.org/10.1016/j.optmat.2016.07.026>.
51. B. Devakumar, P. Halappa, and C. Shivakumara,  $Dy^{3+}/Eu^{3+}$  co-doped  $CsGd(MoO_4)_2$  phosphor with tunable photoluminescence properties for near-UV WLEDs applications. *Dyes Pigm.* 137, 244–255 (2017). <https://doi.org/10.1016/j.dyepig.2016.10.016>.
52. E.F. Schubert, *Light emitting diodes*, 2nd ed., (Cambridge: Cambridge Univ. Press, 2006), p.292.

**Publisher's Note** Springer Nature remains neutral with regard to jurisdictional claims in published maps and institutional affiliations.

Springer Nature or its licensor (e.g. a society or other partner) holds exclusive rights to this article under a publishing agreement with the author(s) or other rightsholder(s); author self-archiving of the accepted manuscript version of this article is solely governed by the terms of such publishing agreement and applicable law.